ACS Catalysis

Research Article

pubs.acs.org/acscatalysis

QM/MM Study and MD Simulations on the Hypertension Regulator Angiotensin-Converting Enzyme

Natércia F. Brás, Pedro A. Fernandes, and Maria J. Ramos*

REQUIMTE, Departamento de Química e Bioquímica, Faculdade de Ciências, Universidade do Porto, Rua do Campo Alegre s/n, 4169-007 Porto, Portugal

Supporting Information

ABSTRACT: Human angiotensin-converting enzyme (ACE) is a zinc metallopeptidase that converts angiotensin I to the vasoconstrictor angiotensin II and inactivates the vasodilator bradykinin. This dual ability is vital to blood pressure regulation and management of hypertension. Despite the many enzymatic studies on zinc metallopeptidases, the correct substrate binding mode and catalysis of ACE are still not completely understood. Two buried chloride ions activate the ACE hydrolysis efficiency in a substrate-dependent manner, but the molecular mechanism associated with this activation also remains unclear. In this work, the catalytic mechanism of ACE was studied with atomistic detail, using a hybrid quantum mechanical/molecular mechanical method at the ONIOM(M06-2X/6-311+G(d,p):Amber//B3LYP/6-31G(d):Amber) level. The hydrolytic reaction proceeds via a general acid/base mechanism, in which the first mechanistic step involves the displacement of the zinc-bound water molecule that performs a nucleophilic attack on the scissile carbonyl bond to form an oxyanion that results in a gem-diol intermediate. The second step involves a proton transfer from Glu384 to the peptide nitrogen and a subsequent cleavage of the peptidic bond to yield the products in their neutral forms. The conserved residue Glu384 is ideally aligned and has the ability to slightly rearrange its conformation to act as a highly effective proton shuttle. Our results indicate that the nucleophilic attack is the rate-limiting step of ACE catalysis (barrier of ≈19 kcal/mol), which agrees with the experimental data available. Molecular dynamics simulations on ACE were also performed, and the data reported here provide a structural basis for the chloride-dependent activity of ACE. It was observed that the Cl2 absence allows a conformational rearrangement of the Arg522 side chain, which subsequently makes an electrostatic interaction with the zinc-bound Glu411 and perturbs the metal center polarization role during catalysis.

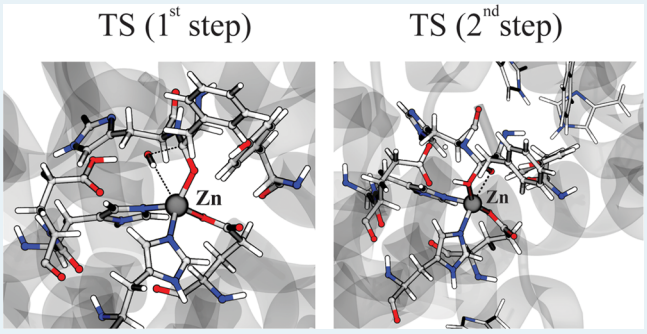

KEYWORDS: *ACE, hypertension, zinc metallopeptidase, QM/MM, Cl-dependence*

INTRODUCTION

Hypertension is a major risk factor in cardiovascular and kidney diseases. Currently, the development of novel therapeutic approaches has focused on the renin−angiotensin−aldosterone system (RAAS) that plays a key role in the regulation of blood pressure and electrolyte balance in humans.[1,2] Angiotensin I-converting enzyme (ACE) is a key enzyme in the RAAS cascade, with a vital role in the metabolism of biologically active peptides. It is a zinc metallopeptidase that catalyzes the cleavage of the C-terminal histidine-leucine dipeptide from angiotensin I to produce the potent vasoconstrictor octapeptide angiotensin II.[2] In addition, it also inactivates the vasodilator bradykinin by catalyzing the cleavage of its C-terminal proline−phenylalanine tail from the nonapeptide hormone. Due to its dual action, ACE inhibitors were one of the first line therapies in hypertensive and cardiovascular disorders for several years.

ACE (EC 3.4.15.1) belongs to the M2 gluzincin family within the MA clan.[3] In humans, there are two isoforms of ACE that are expressed from the same gene in a tissue-specific manner: the 140 kDa somatic form (sACE), which is found in a variety of tissues, and the 77 kDa testicular form (tACE), which is exclusively expressed in germinal cells. sACE consists of two domains (N and C) with high similarity in sequential identity, although they differ in their substrate and inhibitor specificities, chloride dependence, and physiological functions.[4] It was proposed that the C domain is necessary for controlling blood pressure and cardiovascular function, presenting a similar role of the monomeric tACE enzyme. The structure of tACE has an overall ellipsoid shape with a central extended groove that divides the protein into two subdomains, where the active site with the typical HEXXH···E zinc-binding motif of gluzincins is located.[5] This is characterized by two histidines (His383 and His387) and a glutamic acid (Glu411) coordinated to the zinc ion, whereas the fourth position is provided by an acetate ion from the crystallization medium (mimicking a water molecule in the solution structure). It is also expected that the Glu384

Received: January 21, 2014
Revised: June 23, 2014
Published: June 24, 2014

   dx.doi.org/10.1021/cs500093h | ACS Catal. 2014, 4, 2587−2597

residue has a key role during catalysis. The overall ACE sequence is largely different than the other members of the MA clan. However, there is a high sequence and structural similarity between the active sites of ACE, thermolysin and carboxypeptidase, which suggests a potential analogous catalytic mechanism for these enzymes.[6−12] Several theoretical studies have been performed to clarify the catalytic mechanisms of these zinc metallopeptidases.[12−23] Very recently, Zhang and coworkers[12] have suggested that the hydrolytic reaction of ACE proceeds via a general acid−base mechanism with the nucleophilic attack of a water molecule on the carbonyl carbon of the scissile bond. It was proposed that the Zn-coordinated water molecule acts as a proton donor for an adjacent glutamate residue. However, several details remain unclear, such as the exact role of the zinc cation during catalysis or the zinc coordination mode in the ACE−substrate complex. Studies on thermolysin have suggested that the zinc plays a significant role in lowering the pK_a of its coordinated water molecule, and its electrostatic effect would stabilize the carbonyl oxyanion produced in the transition states of the reaction pathway.[2,7] One study on carboxypeptidase also suggests that the transition state for proton transfer from the general base/acid glutamate to the peptide nitrogen (in the second reaction step) is the highest peak in the full energy profile.[21] Blumberger J. et al.[20] have studied the thermolysin mechanism through QM/MM simulations and they proposed that the reaction consists of three distinct steps: a Zn-bound water molecule is deprotonated by a glutamate and attacks the carbonyl bond of the substrate; the protonated glutamate transfers its proton to the amide nitrogen atom, and the peptide bond is broken. A specific and interesting characteristic of zinc metalloenzymes is the high flexibility of zinc coordination due to its fast ligand exchange that can adopt different coordination modes and subsequently makes it an invaluable metal in biological catalysis. Wu and colleagues have performed a structural study[17] that applied a Born−Oppenheimer ab initio QM/MM molecular dynamics simulation in thermolysin and histone deacetylase enzymes, and their data reveal that the catalytic zinc ion in the former can adopt a tetra-, penta-, or hexa-coordination during the picosecond's time scale (involving solvent molecules).[17] The dynamic change in coordination of the carboxylate bound to zinc in the catalytic process, known as carboxylate shift, may help in this zinc-exchange coordination.[24] However, in the histone deacetylase and carboxypeptidase mechanisms, only the monodentate binding mode for the carboxylate coordination was observed.[15,17] All these data clearly indicate that the zinc coordination spheres are quite different within the same class of zinc metalloproteases.

To the best of our knowledge, few computational molecular modeling studies have been performed to characterize different ACE−substrate complexes, in both tetra-coordinated and penta-coordinated zinc configuration.[13,14] However, the ACE catalytic mechanism previously described only considers the tetra-coordinated configuration.[12] Therefore, in this work, a hybrid QM/MM study was performed, to clarify the catalytic mechanism of ACE with atomistic detail, using both tetra-coordinated and penta-coordinated zinc configurations, and taking into account the whole enzyme−substrate complex.

Additionally, it is well-known that chloride ions promote ACE hydrolysis efficiency in a substrate-dependent manner.[25−27] Although the molecular mechanism for Cl^- activation in ACE remains unclear, it was proposed that these anions are responsible for the correct position of residues involved in stabilizing the enzyme−substrate complex or fine-tuning the pK_a of some catalytic residues. Experimental data suggested that they decrease the barrier reaction by 2.5 kcal/mol, which improves ACE catalytic activity.[27] However, a recent study suggests that the absence of chloride does not change the overall free-energy profiles of the ACE catalysis, and the major contribution of Cl^- might come from the possible long-range electrostatic interactions with the substrate, not yet identified.[12] The tACE enzyme has two buried chloride ions outside the active site. One chloride ion is 20.7 Å away from the zinc ion, and it is bound to one water molecule as well as Arg186, Trp486, and Arg489 side chains, maintaining dispersion contacts also with a shell formed by four tryptophan residues. The second chloride ion is ca. 10 Å away from the zinc ion, and it is bound to Tyr224, Arg522 and to a water molecule. The latter arginine has been described to be involved in the chloride dependence of the ACE activity, as its mutation to glutamine led to loss of this dependency.[27] A hydrophobic shell constituted by Pro407, Pro519, and Ile521 residues also surrounds this Cl^- ion. Even though no direct interaction has been established between the second Cl^- ion and the substrate, it is bound to Arg522 that lies in the same helix of the Tyr520 and Tyr523 residues, which interact with the substrate or inhibitors. Previous studies have proposed that this Cl^- ion acts as an ionic switch as its removal disrupts the salt bridge with the positively charged Arg522, which rearranges to interact with Asp465, triggering structural rearrangements on Tyr520 and Tyr523 that move them away from the active site, reducing enzyme affinity to the substrate.[25] Another proposal was put forward showing that, in the absence of Cl^- ions, several intramolecular interactions can occur and turn critical regions of the substrate-binding site poorly accessible to the substrate.[12,26] Therefore, the presence of Cl^- may keep the active site of ACE in a conformation that favors substrate binding. To understand the role of Cl^- in ACE, molecular dynamics simulations in the presence and absence of this anion were performed to clarify the structural rearrangements that take place in the absence of the ion and the basis for the chloride dependency.

These computational approaches proved to be useful in detailing the most plausible catalytic mechanisms of ACE and providing a structural characterization of the dynamic rearrangements on Cl^- binding site. Considering that ACE is essential for blood pressure regulation and electrolyte homeostasis in humans, these data are of great interest for the pharmaceutical industries to guide future studies in developing novel strategies for ACE inactivation.

COMPUTATIONAL METHODS

ACE Catalytic Mechanism. *Molecular Modeling.* A structure of human tACE complexed with the inhibitor enalaprilat (at 1.8 Å resolution) was taken from the protein databank (PDB ID: 1UZE)[5] and used as the starting point for the QM/MM study. The inhibitor was used as template to build the tetrapeptide (Pro7−Phe8−His9−Leu10). All crystallographic water molecules were maintained, and one water molecule was added directly bound to the zinc ion. The hydrogen atoms were added with X-leap,[28] considering all residues in their physiological protonation states. Thirteen counterions (Na^+) were employed to neutralize the negative charge of the system. The X-Leap program was utilized for this purpose. An explicit solvation model with pre-equilibrated TIP3P water molecules was used, filling a truncated octahedral

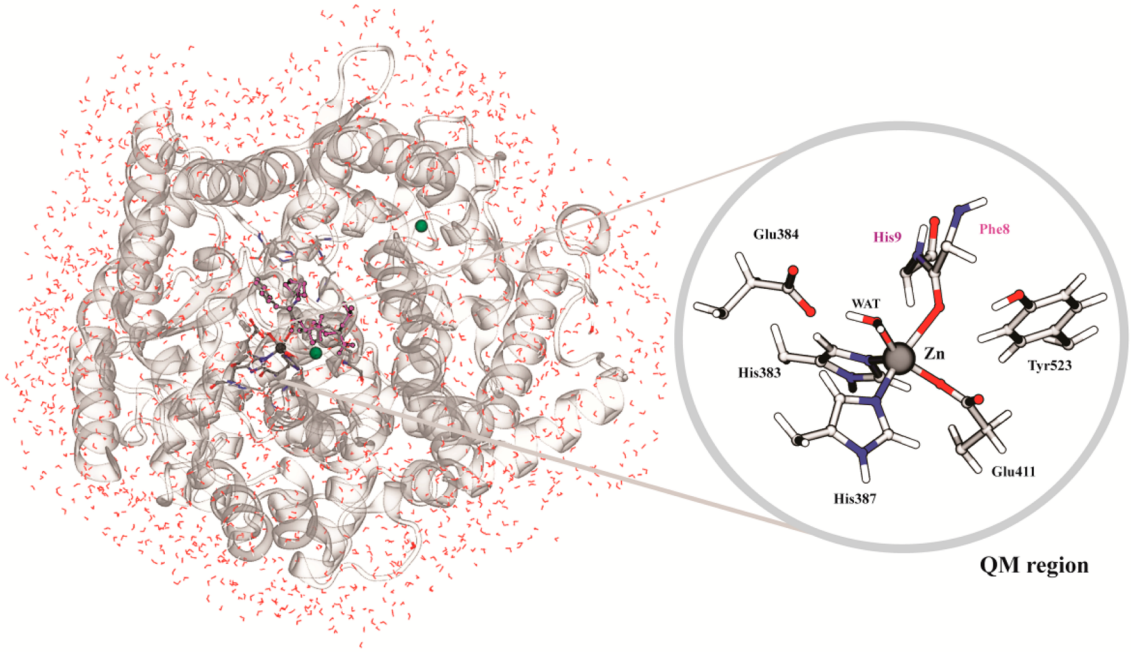

Figure 1. QM/MM model used in the calculations, which included the whole enzyme, the substrate, and a shell of water molecules. The enzyme is colored gray and depicted as a cartoon; the substrate is colored violet and depicted in ball and stick representation; the catalytic residues are depicted in licorice; and the zinc and chloride ions are colored gray and green, respectively. A close-up of the quantum mechanical system is shown on the right-hand side.

box with a minimum distance of 12 Å between the box faces and any atom of the protein. To release the bad contacts in the crystallographic structure, the complex geometry was minimized in two stages: first the protein was kept fixed and only the position of the water molecules and counterions was minimized. Subsequently, the full system was minimized. The optimization procedure was performed with the parametrization adopted in the AMBER 10.0 simulation package,[28] using the Amber 2003 force field (parm03).[29]

QM/MM (ONIOM). The QM/MM calculations performed to determine the potential energy surface (PES) along the catalytic pathway were made with the Gaussian 09 software.[30] We used the optimized structure to build the QM/MM model, in which we included the entire ACE−tetrapeptide system and a water shell with all water molecules within a 5 Å radius of the complex. The system was composed of a total of 14 550 atoms. To explore the PES of the catalytic reaction, our system was divided into two layers, within the ONIOM formalism[31,32] as implemented in the Gaussian 09 package.[30] In geometry optimizations, the high-level layer included the Phe8 and His9 residues of the substrate, the catalytic water molecule, the zinc ion, and the side chains (until the beta carbon) of His383, Glu384, His387, Glu411 and Tyr523 in a total of 71 atoms (please see details about the included atoms in Figure 1), and it was treated with density functional theory (DFT) at the unrestricted B3LYP/6-31G(d) level.[33−35] This density functional was shown to have led to good agreement in the geometries and the activation and reaction energies with higher-level post-Hartree−Fock methods.[36,37] The QM/MM boundaries crossed carbon−carbon bonds, and hydrogen atoms were used as "link" atoms. The rest of the system was treated at the molecular mechanics level with the pam03 force field and the position of water molecules (except the catalytic one) was constrained. For each reaction step, we performed a linear transit scan along the reaction coordinate with a step value of 0.05 Å to locate all the stationary points. This step was reduced to 0.01 Å in the regions of the higher-energy structures, which were considered as a very good approximation to the transition-state geometries.[38,39] The interaction between the layers was described with the electronic embedding scheme that includes the partial charges of the MM region into the QM calculations and allows for polarization of the QM region by the MM charges, providing a better description of the electrostatic interaction between the QM and the MM regions.[40] Using this approach, single-point energy calculations were then performed on the optimized geometries, treating the higher layer at the DFT level, with the B3LYP,[33−35] B3LYP-D3,[33−35,41] X3LYP,[42] B1B95,[33,34] mPWB1K,[43] B97-D,[44] B97−2,[45] BB1K,[33,34,46] M06-L,[47] M06-2X,[48,49] and M05-2X[50] functionals associated with the larger 6-311+G(d,p) basis set. We used these density functionals because they were shown to have led to good agreement in the activation and reaction energies with higher-level post-Hartree−Fock methods,[36] and they were also successfully used and indicated as the most accurate functionals to characterize zinc metallopeptidases.[51−54]

Molecular Dynamics Simulations To Understand the Cl^- Ion Role in ACE Activity. A structure of human tACE (at 2.0 Å resolution) was taken from the protein databank (PDB ID: 1O8A).[5] This unbound ACE structure was used as the starting point for the subsequent MD simulations in order to observe structural changes caused by the absence of the Cl^- anion. The absence of Cl^- may influence the conformation of the active site residues, which in turn may affect substrate binding and catalysis. All crystallographic water molecules were maintained and hydrogen atoms were added with the Amber software X-Leap,[28] taking into account all residues in their physiological protonation state. The catalytic water molecule was modeled from the acetate ion. The parameters of the

dx.doi.org/10.1021/cs500093h | *ACS Catal.* 2014, 4, 2587−2597

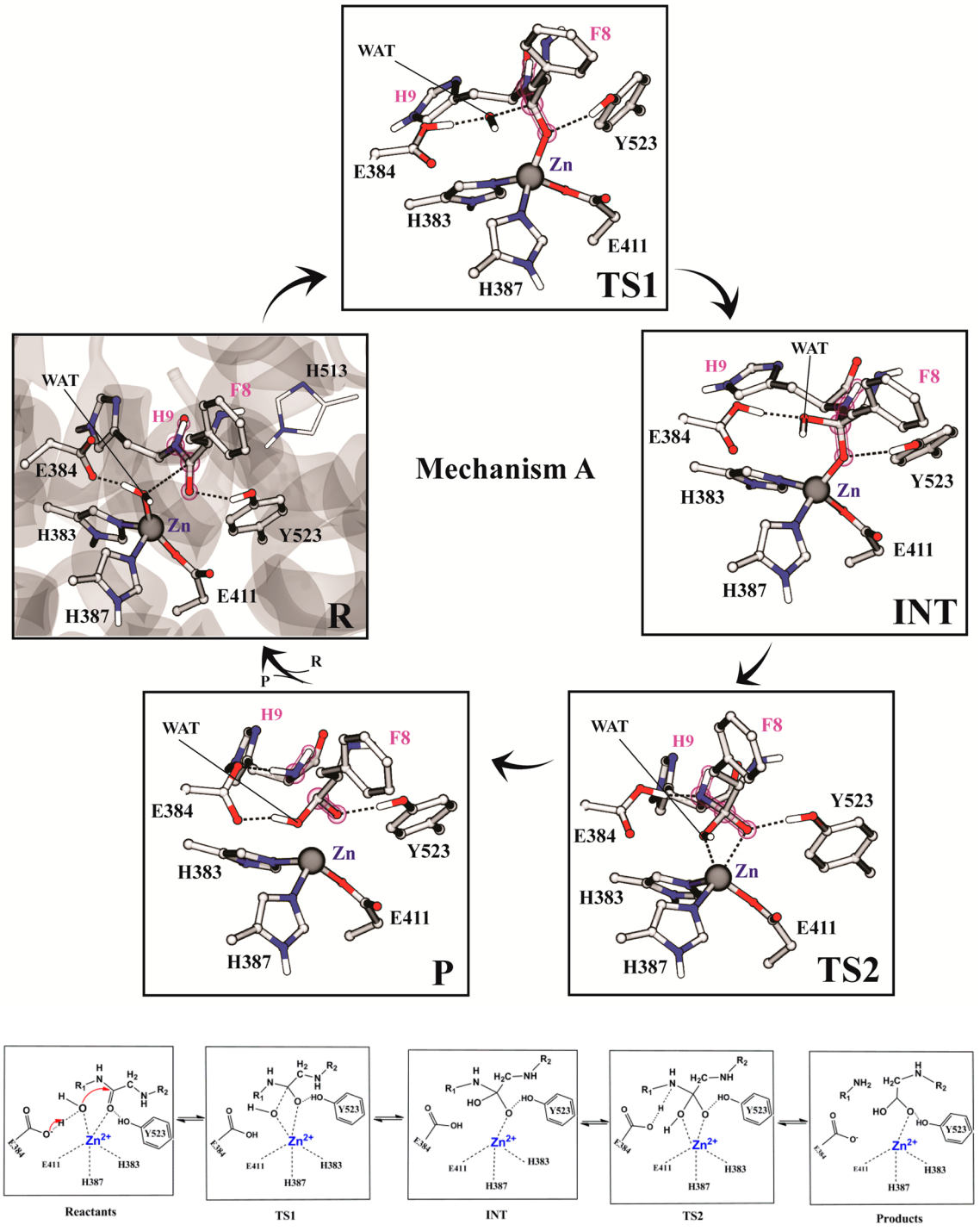

Figure 2. Representation of structure for the reactants ($R_{Mech\text{-}A}$), transition states ($TS1_{Mech\text{-}A}$ and $TS2_{Mech\text{-}A}$), intermediates ($INT_{Mech\text{-}A}$), and products ($P_{Mech\text{-}A}$) of the pentacoordinated catalytic mechanism, emphasizing the main relevant interactions established.

metallic active sphere were determined, and their detailed description is provided in Supporting Information (SI). A semiflexible model approach was used to calculate the force constants for the bond and angles parameters of the zinc center.[55] Electrostatic charges were determined from a RESP fitting of Merz−Kollman charges.[56] Dihedral force constants involving the Zn were set to zero, whereas transferable van der Waals atomic parameters were taken from the literature.[57−59] A detailed description of all MD simulation steps is also presented in SI. All geometry optimizations and MD simulations were performed with the parametrization adopted in AMBER 10.0 simulations package,[28] using the Amber 2003 force field (parm03)[29,60] for the proteins. MD simulations of 100 ps at constant volume and temperature, and considering periodic boundaries conditions were run, followed by 10 ns of MD simulation with an isothermal−isobaric NPT ensemble (constant number of particles, pressure, and temperature) for each system in which Langevin dynamics was used (collision frequency of 1.0 ps^{-1}) to control the temperature at 310.15 K.[61] The MD simulation without the Cl^- ion was repeated three times with different initial velocities to get different paths for the system's evolution. Hydrogen bonds were constrained using

dx.doi.org/10.1021/cs500093h | ACS Catal. 2014, 4, 2587−2597

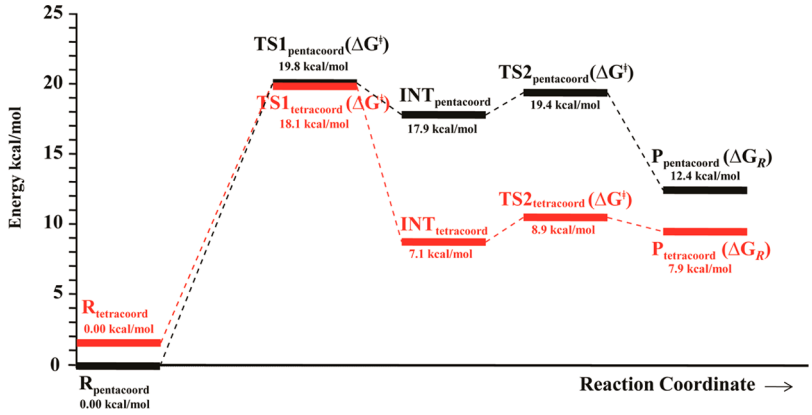

Figure 3. Energetic pathways for the pentacoordinated (black lines) and tetracoordinated (red lines) hydrolysis mechanism of the tetrapeptide substrate (Phe8−His9 peptidic bond) catalyzed by ACE at the ONIOM(M06-2X/6-311+G(d,p):Amber//B3LYP/6-31G(d):Amber) level.

the SHAKE algorithm,[62] and the particle−mesh Ewald method[63] was used to include the long-range interactions.

RESULTS AND DISCUSSION

ACE Catalytic Mechanism Study. Even though ACE is one of the most important targets for drug design to control hypertension, its catalytic mechanism has not been completely clarified. Until now, it has been indicated that the reaction mechanism of ACE occurs by a general base−general acid mechanism,[12] like other monozinc metallopeptidases such as thermolysin, carboxypeptidase, β-lactamases, and histone deacetylases. However, despite the availability of extensive experimental and theoretical studies on various zinc-dependent enzymes, there is still no agreement about the specific details involved on the ACE catalytic activity. To investigate the energetics and the paths associated with the most favored mechanism, we have computed the potential energy surface at the QM/MM level of theory.

ACE Catalytic Mechanism A (Mech-A) Starting with a Zn-Pentacoordinated ACE/Substrate Complex. The initial structure for a QM/MM simulation of the enzyme−substrate (ES) was modeled from X-ray ACE−enalaprilat inhibitor structure where one oxygen atom of its carboxylate group is bound to the metal ion. Considering the small size of the inhibitor, only the last tetrapeptide (Pro7−Phe8−His9−Leu10) of the native substrate was built, which binds in a highly ordered extended conformation but does not entirely occupy the large space inside the catalytic groove of ACE (Figure 1).

Upon complex formation, no significant rearrangement of active site residues was observed after energy optimization. The benzene group of Phe8 at the S1 site is accommodated in a hydrophobic pocket formed by Phe512 and Val518. The C-terminal carboxylate of the substrate is stabilized by a hydrogen bond to Gln281 (3.20 Å), whereas the Ala354 backbone oxygen is also H-bonded to the scissile bond nitrogen of the substrate (1.90 Å). In addition, the substrate backbone carbonyl groups are hydrogen bonded to His353 (1.91 Å), His513 (2.70 Å), and Tyr523 (2.04 Å). Although all these residues are important, the latter is noticeably crucial due to its catalytic effect in the stabilization of reactants by its interaction with the scissile bond carbonyl oxygen. It was also verified that the incoming tetrapeptide optimizes its interactions in the active site and only slightly displaces the catalytic water toward Glu384 (O_w−Zn distance of 2.04 Å). This improves the nucleophilicity of the water oxygen to promote attack on the scissile carbonyl carbon of the substrate due to polarization provided by the carboxylate group. Because in the reactants (R_{Mech-A}) the substrate carbonyl group binds directly to the zinc ion (CO−Zn distance of 2.37 Å), this direct coordination allows the polarization of the carbonyl group, making it more susceptible to nucleophilic attack. The distance between the reactive water molecule and the carbonyl carbon atom is 3.09 Å. Along with the nucleophilic attack, a concerted proton transfer was verified, and at a O_w−CO distance of 2.12 Å, the water proton is fully transferred to Glu384 and remains strongly hydrogen-bonded to the reactive hydroxide ion (1.57 Å). Figure 2 shows the geometries for the reactants, transition states, intermediates, and products obtained for this catalytic mechanism. In the first transition state ($TS1_{Mech-A}$), the substrate is strongly bonded to Zn (CO−Zn = 1.95 Å), whereas the hydroxide is displaced from the Zn sphere (O_w−Zn = 3.10 Å). The electrostatic effect of the Zn ion stabilizes the negative charge on the carbonyl oxyanion in the $TS1_{Mech-A}$, which is also stabilized by the strong H-bond between this group and the hydroxyl group of Tyr523 (2.08 Å). This first mechanistic step results in the formation of a tetrahedral intermediate (INT_{Mech-A}), with the three protein ligands (His383, His387, and Glu411) and the carbonyl group of the substrate strongly bonded to the zinc ion (1.93 Å). As shown in Figure 2, the $TS1_{Mech-A}$ and INT_{Mech-A} geometries are very similar, which is in accordance with their analogous energies. Following this, in the second step, the proton accepted by Glu384 is shuttled to the scissile nitrogen group that results in the cleavage of the peptidic C−N bond and the product release. However, the orientation of Glu384 is unfavorable to directly transfer its proton to the substrate amine group. To overcome this, a stereochemical rearrangement of its conformation occurs along the potential energy surface of this step to facilitate the proton moving to the leaving group. The second transition state ($TS2_{Mech-A}$) is characterized by H−N and N−C distances of 1.59 and 1.50 Å respectively, culminating in the products (P_{Mech-A}). These were released in their neutral forms (NH_2 and COOH), and the terminal protonated carboxylate is stabilized by a Tyr523 H-bond of 1.78 Å. As expected, it was confirmed that this tyrosine residue plays a crucial role during the entire reaction by stabilizing the carbonyl group of the substrate. Another key catalytic residue is His513 because of its strategic position in both transition-state geometries of this mechanism. It makes H-bonds with the HO-Tyr523 group, carbonyl and amine groups of Pro7 and Phe8 of substrate, stabilizing these geometries and the tetrahedral

dx.doi.org/10.1021/cs500093h | ACS Catal. 2014, 4, 2587−2597

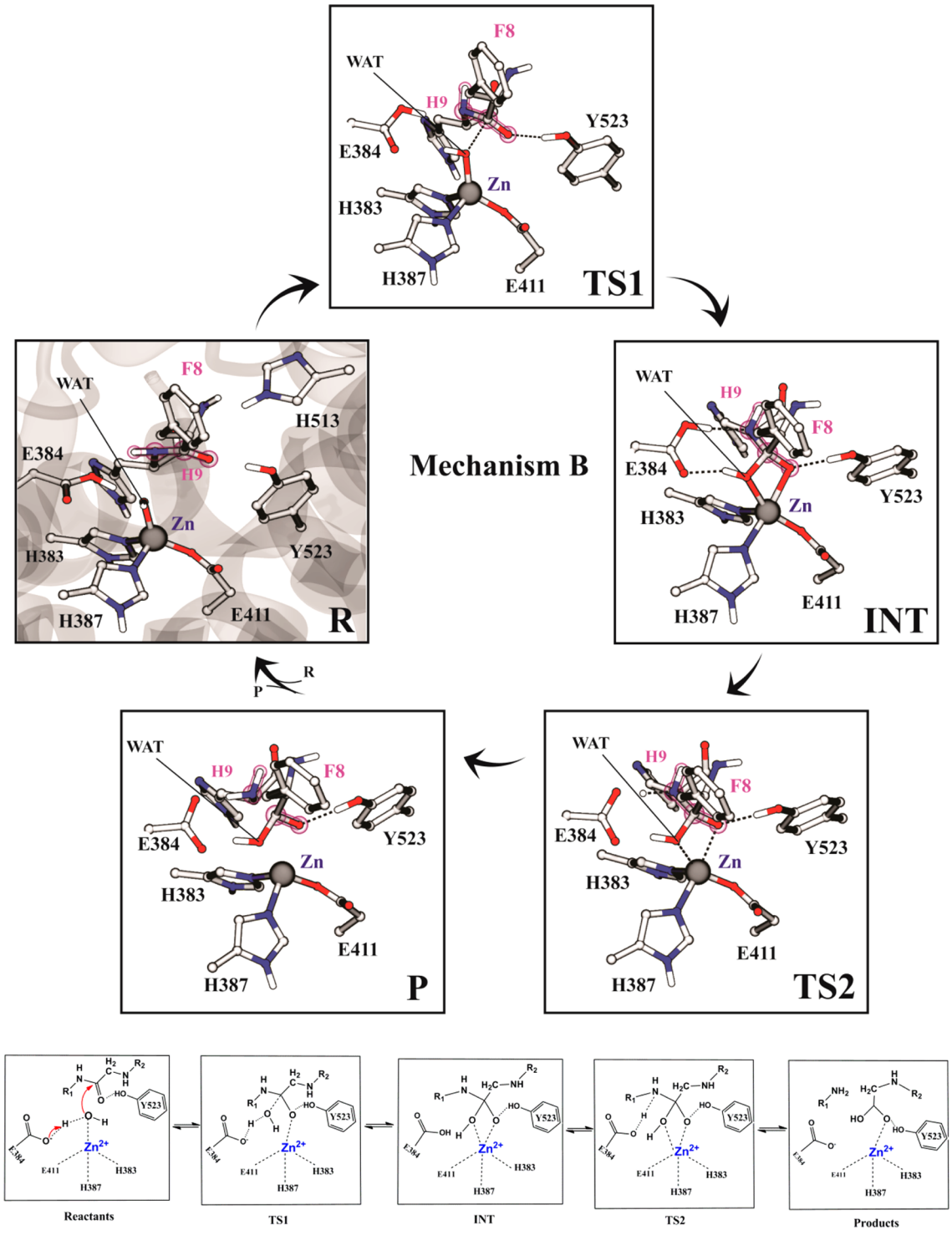

Figure 4. Representation of structures for the reactants ($R_{Mech\text{-}B}$), transition states ($TS1_{Mech\text{-}B}$ and $TS2_{Mech\text{-}B}$), intermediates ($INT_{Mech\text{-}B}$), and products ($P_{Mech\text{-}B}$) of the tetracoordinated catalytic mechanism, emphasizing the most crucial interactions established.

intermediate. The observed H-bond net is consistent and agrees with a previous experimental study, in which the His513 mutation by Ala or Leu residues decreases the barrier by 3.74 or 5.13 kcal/mol, as a result of the loss of strong H-bonds in the tetrahedral intermediate.[64,65]

Figure 3 shows the energetic profile obtained at the ONIOM(M06-2X/6-311+G(d,p):Amber//B3LYP/6-31G-(d):Amber) level. The barriers correspond to electronic energies, instead of Gibbs activation energies, because it was not possible to calculate zero point energy (ZPE) values and vibrational entropies in such a large and partially frozen system. This is a common procedure in the computational studies of catalytic mechanisms with large enzymatic models. Other mechanistic studies (including protease enzymes) have shown that the contribution from ZPE and entropy is relatively small, lowering the TS energies by approximately 1−2 kcal/mol).[66−69] The calculated activation barrier for formation of the tetrahedral intermediate is 19.8 kcal/mol, and this step is

dx.doi.org/10.1021/cs500093h | ACS Catal. 2014, 4, 2587−2597

endergonic by 17.9 kcal/mol, whereas the second step is characterized by a barrier of 19.4 kcal/mol. These values agree with the experimental barrier of ACE catalysis.[64] Despite the rate-limiting step being the first one, the small difference between the nucleophilic attack and protonation of the leaving group barriers suggests that the two mechanistic steps occur sequentially with comparable rates.

Furthermore, it was also shown that along the catalysis process, the zinc coordination fluctuates between five and four ligands, and its main flexibility comes from the binding of the water molecule. The pentacoordinated Michaelis complex of ACE presented here differs from another proposed by Sturrock et al.,[2] in which the water is not zinc-bound and the fourth ligand of the metal center is the substrate carbonyl oxygen atom. In addition, this also contrasts with the one proposed by Zhang et al.,[12] in which the zinc ion is tetracoordinated in its active site. However, several enzymes possess a zinc ion in the pentacoordinated state, in their metallic centers, and other studies suggest that the binding of substrate to Zn in the ES structure is the most usual for zinc metallopeptidases because the substrate and the water molecule are almost perfectly aligned for nucleophilic attack.[20] Recently, the ES complex of ACE was modeled by Papakyriakou et al.[13] as a pentacoordinated species (both the nucleophilic water and substrate carbonyl oxygen are zinc-bound), and this coordination was maintained during the MD simulations with the peptide substrate GnRH.

ACE Catalytic Mechanism B (Mech-B) Starting with a Zn-Tetracoordinated ACE/Substrate Complex. In the tetracoordinated mechanism generally accepted for several zinc metallopeptidases, it is considered that when the substrate enters in the binding site, its neutral carbonyl oxygen atom does not interact strongly with the zinc ion, and it is unlikely to dislodge the zinc-bound water. Considering that the ACE mechanism recently studied involves a tetracoordinated metal center, analogous to thermolysin, a similar ACE−substrate complex was built too. These new reactants ($R_{Mech\text{-}B}$) were obtained from $R_{Mech\text{-}A}$ through the exit of the carbonyl oxygen atom from the first metal coordination sphere. Figure 4 shows the reactants, transition states, intermediates and products geometries obtained for this mechanism (Mech-B). It was observed that in these reactants, the CO−Zn distance is 4.36 Å and the remaining ligands (catalytic water, His383, His387, and Glu411) are tightly bound to the Zn ion, forming a 4-fold coordination sphere. In this rearrangement, the Glu384 acts as the general base, activating the catalytic zinc-bound water via a spontaneous proton transfer, and the remaining hydroxide strongly interacts with the metal ion (1.92 Å). This geometry is in agreement with previous studies on ACE performed by Wang et al.[14] and Zhang et al.,[12] in which the tripeptide substrate has no direct contact with the zinc ion (4.51 ± 0.36 Å), and the water molecule is 2.04 ± 0.06 Å from the zinc ion in the reactants state. As seen in Figure 4, the interaction of the substrate with the enzyme only occurs via a network of hydrogen bonds, and the metal cofactor does not play a significant role in polarizing the substrate carbonyl group. In the tetracoordinated ES complex, the zinc-bound hydroxide group is located in a near-attack configuration, with a distance of 3.23 Å. Similarly to the previous ACE Mech-A, in the first step, the hydroxide group attacks the peptide carbonyl carbon, and as the reaction proceeds, a tight bond between the substrate and the Zn is formed, resulting in a gem-diol intermediate ($INT_{Mech\text{-}B}$). This is characterized by an sp3 central carbon and a O_w−Zn and O−Zn distances of 2.13 and 2.12 Å respectively. The first transition state ($TS1_{Mech\text{-}B}$), represented in Figure 4, is characterized by a weak bond, established between the substrate and the zinc ion (3.25 Å), whereas the hydroxide group is becoming bound to the metal (1.88 Å) and closer to the carbonyl carbon (2.13 Å). The central C atom distorts away from its planar geometry in ES. The stabilization of this $TS1_{Mech\text{-}B}$ is achieved through the establishment of an H-bond established between the carbonyl oxygen atom of the substrate and the OH group of Tyr523 (1.79 Å). In the second step, the protonated carboxylate of Glu384 slightly rotates its conformation and forms an H-bond with the scissile NH group of the substrate. This small rearrangement puts this residue correctly positioned to transfer its proton to the nitrogen atom. As shown in Figure 4, the second transition state ($TS2_{Mech\text{-}B}$) is characterized by H−N and N−C distances of 1.38 and 1.55 Å respectively. The final products were released in their neutral forms (NH_2 and COOH), and the terminal protonated carboxylate group is stabilized by a Tyr523 H-bond of 1.78 Å. In addition to Tyr523, the His513 also plays a key role along the reaction due to its stabilization of transition-state geometries promoted by the establishment of H-bonds with the carbonyl and amine groups of residues Pro7 and Phe8 of the substrate. As occurred previously, in the Mech-B, the coordination number of the zinc ion varies between 4 and 5 in the first and second mechanistic steps. However, in this case, the main flexibility comes from the coordination of the substrate. A similar tetracoordinated catalytic mechanism has been established computationally for ACE with another substrate, the tripeptide hippuryl−histidine−leucine. The QM/MM methodology employed by Zhang and co-workers[12] use a semiempirical approach (SCC-DFTB) to describe the region where the chemical reaction occurs. This Hamiltonian is clearly less accurate than the one used here. However, they have done conformational sampling, which we cannot carry out with our Hamiltonian. Hence, our methods are complementary. It is also important to highlight that their data are comparable with our Mech-B results, which give confidence in the ACE mechanistic pathway, as well as validate and reinforce the correctness of the theoretical methods employed.

Furthermore, analogous tetracoordinated mechanisms of action have been established computationally for thermolysin and carboxypeptidase, and the resulting barriers are consistent with kinetic data for these enzymes. However, for carboxypeptidase, it was also proposed that the "anhydride mechanism",[16] in which a direct nucleophilic attack on the peptide carbonyl group by a general base glutamate (Glu384 in ACE), results in the formation of an anhydride intermediate that is subsequently hydrolyzed by water to form the product. In ACE, this hypothesis was not considered because stereochemical restrictions of the X-ray Glu384 position make a direct nucleophilic attack by this residue to the carbonyl group of the substrate very unlikely.

The energetic profile obtained at the ONIOM(M06-2X/6-311+G(d,p):Amber//B3LYP/6-31G(d):Amber) level for the Mech-B is also shown in Figure 3. The calculated barrier for the formation of the gem-diol intermediate is 18.1 kcal/mol, whereas the second step is characterized by a barrier of 8.9 kcal/mol. These barrier values are in good agreement with the experimental Gibbs activation energy for Ang I hydrolysis by the human ACE C-domain that is 16.4 kcal/mol.[64] Comparing the energies of both ES complexes ($R_{Mech\text{-}A}$ and $R_{Mech\text{-}B}$), we

dx.doi.org/10.1021/cs500093h | ACS Catal. 2014, 4, 2587−2597

Table 1. Activation and Reaction Enthalpy Energies Obtained for Both ACE Mechanisms[a]

	Mech-A				Mech-B			
functional	TS1 ($\Delta G^{\ddagger}$)	INT1	TS2 ($\Delta G^{\ddagger}$)	P (ΔG_R)	TS1 ($\Delta G^{\ddagger}$)	INT1	TS2 ($\Delta G^{\ddagger}$)	P (ΔG_R)
B3LYP	23.1	23.0	30.2	18.9	21.7	20.5	22.5	19.5
B3LYP-D3	21.1	22.1	25.8	13.3	18.5	15.1	15.9	12.7
X3LYP	22.8	22.9	29.4	18.1	20.8	19.5	21.4	18.5
B97-D	18.7	21.1	24.5	13.7	18.3	17.0	17.1	15.3
B97−2	22.8	21.9	28.6	18.5	21.3	18.7	20.9	18.2
B1B95	20.2	19.0	24.7	15.5	19.3	13.6	16.0	13.5
mPWB1K	20.8	18.2	23.4	15.7	19.3	10.5	13.7	11.1
M06-L	19.3	20.9	23.4	14.2	16.7	13.3	15.8	13.2
M06-2X	19.8	17.9	19.4	12.4	18.1	7.1	8.9	7.9
M05-2X	18.9	17.3	20.3	12.2	18.7	9.1	10.8	9.1

[a]QM region treated at the B3LYP, B3LYP-D3, X3LYP, B97-D, B97-2, B1B95, mPWB1K, M06-L, M06-2X, and M05-2X density functionals, using the 6-311+G(d,p) basis set and the electrostatic embedding scheme.

observed that the reactants with 5-fold zinc coordination are energetically more stable (−1.64 kcal/mol), which suggests that although both metal-coordination structures exist, the ACE catalysis should start mostly from the Zn-pentacoordinated structure. However, the energetic profile of Mech-B is more favorable and closer to the experimental values. Considering the two energetic profiles, we suggest that both catalytic mechanisms (Mech-A and Mech-B) may possibly occur, with a slight preference for Mech-B. According to these results, the nucleophilic attack is the rate-limiting step for the ACE catalytic mechanism. We also noticed that the total reaction is endergonic, which is understandable and may be related to the difficulty for the products to leave because the ACE active site is located in a very narrow extended groove between the two subdomains (as shown in Figure 1). Probably the whole cycle will be exoenergetic if we take product dissociation into account.

It is well-known that DFT results might depend on the specific functional used in the calculations. To check this influence on the present ACE results, several density functionals successfully applied in other zinc metallopeptidases studies,[37,51−54] were used to repeat the PES. Table 1 shows the activation and reaction energies obtained for additional single-point energy calculations performed on all optimized QM/MM geometries with the electronic embedding scheme, and treating the high level with the B3LYP, B3LYP-D3, X3LYP, B97-D, B97−2, B1B95, mPWB1K, M06-L, M06-2X, and M05-2X density functionals associated with the larger 6-311+G(d,p) basis set. We noticed that B3LYP shows the highest energy values, which is uncommon because B3LYP is known to underestimate barriers. The barriers obtained for the other density functionals are similar. It was verified that the inclusion of the dispersion effects in the B3LYP functional, decrease both barriers by approximately 2 kcal/mol. The role for dispersion in lowering the barrier is small but significant, which is important both in terms of catalysis and also from a methodological point of view. This fact reinforces the already recognized importance of dispersion effects in modeling enzyme-catalyzed reactions with density functional theory methods.[70,71] The B97-D, M06-L, M05-2X, and M06-2X density functional show the lowest activation energies for the first step in both Mech-A and Mech-B mechanisms. These barriers are also the closer values to the activation energies obtained experimentally, which suggest that these four density functionals reproduce accurately the energetic profile of the ACE mechanism of action and lead to exactly the same catalytic mechanism. Hence, they could be employed in the study of other zinc metalloproteins. In general, they overestimate the experimental activation enthalpy by 1−3 kcal/mol. The slight differences likely originate from the smaller substrate used (tetrapeptide instead the native octapeptide) and from the use of enthalpic barriers instead of the activation Gibbs energies (note that vibrational entropy lowers the barriers). However, this difference is included in the error associated with the procedure, and our computed results can be considered as in very good agreement with existing experimental data.

Chloride Role in the ACE Activity. The ACE has two buried chloride ions outside the active site, and earlier experimental studies suggested that the second chloride ion is crucial for its enzymatic activity. This ion makes a direct salt bridge with Arg522, and the mutation of this residue to a glutamine led to a loss of this dependence.[27] It was proposed that in the absence of Cl^-, the positively charged Arg522 changes its conformation to electrostatically interact with Asp465, triggering structural movements on Tyr520 and Tyr523 residues away from the active site that subsequently reduces the enzyme affinity to the substrate. To clarify the molecular mechanism associated with the chloride dependence for ACE catalysis, MD simulations of 10 ns with (ACE_Cl^-) and without Cl^- were performed. Three individual simulations starting from different initial velocities were performed to increase the sampling and evaluate different paths of the system in the absence of Cl^- (ACE_noCl^--1, ACE_noCl^--2, and ACE_noCl^--3). The protein backbone root-mean-square deviation (RMSD) values from the initial structures were obtained for each simulation and are shown in Figure S1 in SI. The RMSD values range between 1.0 and 2.0 Å during the MD simulations, and the overall folding and secondary structural elements are stable, revealing that equilibration of each protein system was achieved. The equilibration of the ACE_noCl^--2 system has required a larger MD simulation (20 ns) to check for longer time scale convergence. Figure S2 in SI illustrates the variation of the radius of gyration (R_g) for each MD simulation. Although all trajectories underwent periodic fluctuations in their R_g values, the overall data indicates that all systems were equilibrated and converged. However, only the last 6 ns were considered in the subsequent distances analysis. According to the root-mean-square fluctuation (RMSF) values by residue obtained for each system (Figure S3 in SI), the residues belonging to ACE loops are those that mostly fluctuate during all the studied simulations, and they are the most flexible regions of the ACE enzyme.

dx.doi.org/10.1021/cs500093h | ACS Catal. 2014, 4, 2587−2597

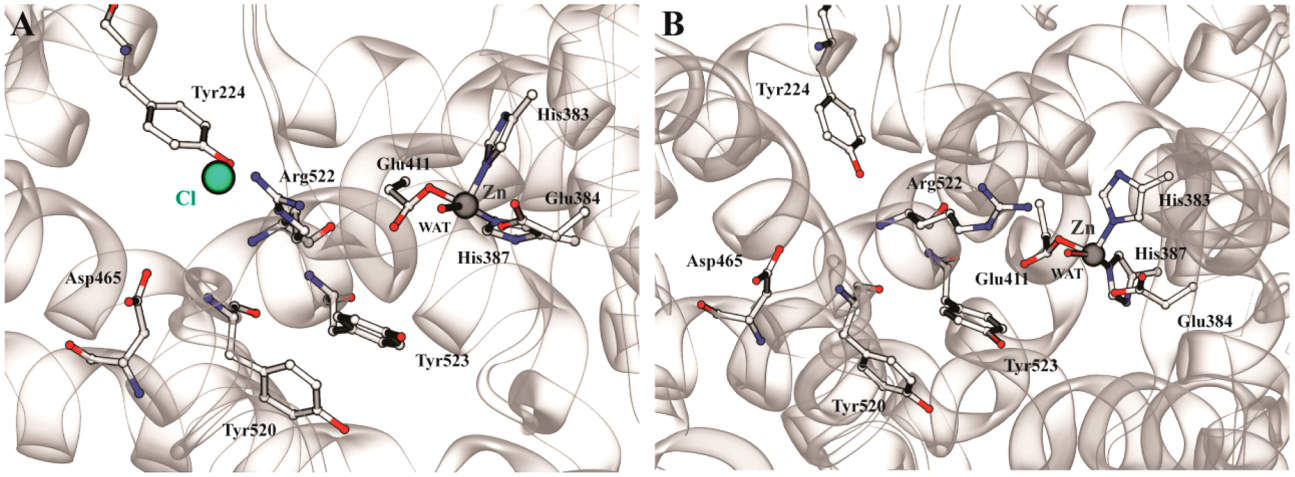

Figure 5. Structural overview around the Arg522 residue in the closest average structures in the presence (A) and absence (B) of Cl^- ion.

Figure 5 shows a structural overview around Arg522 taken from a snapshot at 4 ns of the simulations with and without Cl^- ion (ACE_Cl^- and ACE_noCl^--1 systems). The structures shown in this snapshot are representative of the structure of the enzyme around the Cl^- binding site, which remains stable for the rest of simulations. Similar representations for ACE_noCl^--2 and ACE_noCl^--3 systems are present in Figure S2 in SI. Globally, no major structural rearrangements were observed in the ACE_Cl^- system, and the average distance between the Arg522 residue and the Cl^- ion was 2.44 ± 0.14 Å, which confirms the establishment of a strong salt bridge along the MD simulation. In addition, the average distances between Arg522 and Asp465 and to the catalytic Glu411 were 7.04 ± 0.31 Å and 5.44 ± 0.51 Å, respectively, indicating a large distance between the positively charged residue and both carboxylate groups. In the ACE_noCl^--1 system, the absence of Cl^- ions disrupts the salt bridge with Arg522, and a side chain rotation of the latter residue was observed. This rearrangement allows its approximation and subsequent interaction with the catalytic Glu411 that is directly bound to the zinc ion (distance changes from 4.10 Å to 2.90 ± 0.22), which disturbs the polarization promoted by the metallic center residues and may partially occupy the binding groove, decreasing the ACE affinity for certain substrates. Figure S3 in SI shows the superimposition between the $R_{Mech\text{-}A}$ structure used in the QM/MM study with the structure closest to the average in the ACE_noCl^--1 system, in which rotations of Glu411 and Arg522 side chains were observed. An NH_2 group of Arg522 occupies the substrate pocket binding, and a stereochemical clash between both molecules is evident. These results contrast with those proposed in the literature, as we observed that the Arg522 does not move toward Asp465 (distance varies from 8.50 Å to 10.17 ± 0.49 Å), and the Tyr520 and Tyr523 conformations remain in the same position along the MD simulation. Figure S4 in SI shows these two distances for the three systems without Cl^-, and a very similar behavior was observed in the other systems (ACE_noCl^--2 and ACE_noCl^--3), which corroborate the previous structural analysis.

According to previous experimental activity assays on ACE, the absence of chloride ions increases the binding of angiotensin I and also increases the activation energy required for catalysis.[27] The present MD simulations also suggest that the conformational change may justify chloride dependency in a substrate-specific manner, as certain rearrangements may allow the binding of some substrates over others. In summary, the presence of Cl^- avoids the electrostatic interaction between Arg522 and the zinc-bound Glu411, not interfering in the catalytic role of the zinc metal center.

CONCLUSIONS

ACE is a well-known zinc metalloenzyme involved in blood pressure regulation and as a major target for cardiovascular disease therapy, but its catalytic mechanism is not completely understood.

Our QM/MM calculations indicate that the ACE enzymatic reaction proceeds via a promoted-water pathway with the Glu384 serving as the general base and general acid residue, which is supported by many crystallographic and biochemical studies. The present data indicate that, in the Mech-A catalytic mechanism (starting from a pentacoordinated zinc center), the key roles of the zinc cofactor are the activation of the nucleophilic water molecule, as well as the stabilization and polarization of the substrate carbonyl oxygen atom during the formation of the intermediate. However, starting from reactants with a tetracoordinated zinc ion (Mech-B), the metal cofactor only serves as a Lewis acid to activate the catalytic water and to stabilize the transition states. Tyr523 is an important residue during catalysis because it is responsible for the polarization of the substrate carbonyl and it is also a favorable oxyanion hole to the gem-diolate.

In conclusion, it was shown that the Glu384-assisted water mechanism is energetically feasible and has an energy barrier that is slightly higher but still close to the effective barrier calculated from experimental measurements. We suggested that the ACE catalysis starts with a 5-fold zinc coordination sphere and follows on to a tetracoordinated gem-diol intermediate that falls to a pentacoordinated $INT_{Mech\text{-}B}$ structure. The second step proceeds to a pentacoordinated $TS2_{Mech\text{-}B}$ that culminates in the $P_{Mech\text{-}B}$. Our results also indicate that the first step is the rate-limiting one. This QM/MM study allows for a complete comprehension of the ACE catalytic mechanism with atomistic detail.

Furthermore, the present MD simulations also identify the Cl^- ion role for the ACE chloride dependence because a significant conformational rearrangement of Arg522 side chain was observed in the ion absence. This positive residue establishes an electrostatic interaction with the carboxylate

dx.doi.org/10.1021/cs500093h | ACS Catal. 2014, 4, 2587−2597

group of Glu411 that is bound to the zinc ion and disturbs the metal center polarization during catalysis.

All this knowledge is important for the development of new therapeutic inhibitors in drug design research because it will help to improve and synthesize new antihypertensive drugs for pharmaceutical industries.

■ ASSOCIATED CONTENT

Supporting Information

Computational methods, equilibrium bond-stretching and angle-bending parameters, radius of gyration values, RMSD and RMSF values, structural models, distances between component residues. This material is available free of charge via the Internet at http://pubs.acs.org.

■ AUTHOR INFORMATION

Corresponding Author

*E-mail: mjramos@fc.up.pt.

Notes

The authors declare no competing financial interest.

■ ACKNOWLEDGMENTS

The authors would like to acknowledge the program FEDER/COMPETE and the Fundação para a Ciência e Tecnologia (FCT) for financial support (Projects Pest-C/EQB/LA0006/2013, PTDC/QUI-QUI/121744/2010 and EXCL/QEQ-COM/0394/2012).

■ REFERENCES

(1) Bras, N. F.; Fernandes, P. A.; Ramos, M. J. *Phys. Chem. Chem. Phys.* **2012**, *14*, 12605−12613.

(2) Sturrock, E. D.; Natesh, R.; van Rooyen, J. M.; Acharya, K. R. *Cell. Mol. Life Sci.* **2004**, *61*, 2677−2686.

(3) Gomis-Ruth, F. X. *Crit Rev. Biochem Mol. Biol.* **2008**, *43*, 319−345.

(4) Anthony, C. S.; Corradi, H. R.; Schwager, S. L. U.; Redelinghuys, P.; Georgiadis, D.; Dive, V.; Acharya, K. R.; Sturrock, E. D. *J. Biol. Chem.* **2010**, *285*, 35685−35693.

(5) Natesh, R.; Schwager, S. L. U.; Sturrock, E. D.; Acharya, K. R. *Nature* **2003**, *421*, 551−554.

(6) Guy, J. L.; Jackson, R. M.; Acharya, K. R.; Sturrock, E. D.; Hooper, N. M.; Turner, A. J. *Biochemistry* **2003**, *42*, 13185−13192.

(7) Matthews, B. W. *Acc. Chem. Res.* **1988**, *21*, 333−340.

(8) Vickers, C.; Hales, P.; Kaushik, V.; Dick, L.; Gavin, J.; Tang, J.; Godbout, K.; Parsons, T.; Baronas, E.; Hsieh, F.; Acton, S.; Patane, M.; Nichols, A.; Tummino, P. *J. Biol. Chem.* **2002**, *277*, 14838−14843.

(9) Cummins, P. M.; Pabon, A.; Margulies, E. H.; Glucksman, M. J. *J. Biol. Chem.* **1999**, *274*, 16003−16009.

(10) Christianson, D. W.; Lipscomb, W. N. *Acc. Chem. Res.* **1989**, *22*, 62−69.

(11) Martin, M. T.; Holmquist, B.; Riordan, J. F. *J. Inorg. Biochem.* **1989**, *36*, 39−50.

(12) Zhang, C.; Wu, S.; Xu, D. *J. Phys. Chem. B* **2013**, *117*, 6635−6645.

(13) Papakyriakou, A.; Spyroulias, G. A.; Sturrock, E. D.; Manessi-Zoupa, E.; Cordopatis, P. *Biochemistry* **2007**, *46*, 8753−8765.

(14) Wang, X. M.; Wu, S. S.; Xu, D. G.; Xie, D. G.; Guo, H. *J. Chem. Inf. Model* **2011**, *51*, 1074−1082.

(15) Xu, D. G.; Guo, H. *J. Am. Chem. Soc.* **2009**, *131*, 9780−9788.

(16) Vardi-Kilshtain, A.; Shoham, G.; Goldblum, A. *Mol. Phys.* **2003**, *101*, 2715−2724.

(17) Wu, R. B.; Hu, P.; Wang, S. L.; Cao, Z. X.; Zhang, Y. K. *J. Chem. Theory Comput.* **2010**, *6*, 337−343.

(18) Kilshtain, A. V.; Warshel, A. *Proteins* **2009**, *77*, 536−550.

(19) Diaz, N.; Suarez, D. *J. Phys. Chem. B* **2008**, *112*, 8412−8424.

(20) Blumberger, J.; Lamoureux, G.; Klein, M. L. *J. Chem. Theory Comput.* **2007**, *3*, 1837−1850.

(21) Alvarez-Santos, S.; Gonzalez-Lafont, A.; Lluch, J. M.; Oliva, B.; Aviles, F. X. *New J. Chem.* **1998**, *22*, 319−325.

(22) Pelmenschikov, V.; Blomberg, M. R. A.; Siegbahn, P. E. *J. Biol. Inorg. Chem.* **2002**, *7*, 284−298.

(23) Chen, S.-L.; Marino, T.; Fang, W.-H.; Russo, N.; Himo, F. *J. Phys. Chem. B* **2008**, *112*, 2494−2500.

(24) Sousa, S. F.; Fernandes, P. A.; Ramos, M. J. *J. Am. Chem. Soc.* **2007**, *129*, 1378−1385.

(25) Tzakos, A. G.; Galanis, A. S.; Spyroulias, G. A.; Cordopatis, P.; Manessi-Zoupa, E.; Gerothanassis, I. P. *Protein Eng.* **2003**, *16*, 993−1003.

(26) Pokhrel, R.; McConnell, I. L.; Brudvig, G. W. *Biochemistry* **2011**, *50*, 2725−2734.

(27) Liu, X. F.; Fernandez, M.; Wouters, M. A.; Heyberger, S.; Husain, A. *J. Biol. Chem.* **2001**, *276*, 33518−33525.

(28) Case, D. A.; Darden, T. A.; Cheatham, T. E., III ; Simmerling, C. L.; Wang, J.; Duke, R. E.; Luo, R.; Crowley, M., Walker, R. C. ; Zhang, W.; Merz, K. M.; Wang, B.; Hayik, S.; Roitberg, A.; Seabra, G.; Kolossváry, I.; Wong, K. F., Paesani, F.; Vanicek, J.; Wu, X.; Brozell, S. R.; Steinbrecher, T.; Gohlke, H.; Yang, L.; Tan, C.; Mongan, J.; Hornak, V.; Cui, G.; Mathews, D. H.; Seetin, M. G.; Sagui, C., Babin, V.; Kollman, P. A. AMBER 10, University of California: San Francisco, 2008.

(29) Duan, Y.; Wu, C.; Chowdhury, S.; Lee, M. C.; Xiong, G. M.; Zhang, W.; Yang, R.; Cieplak, P.; Luo, R.; Lee, T.; Caldwell, J.; Wang, J. M.; Kollman, P. *J. Comput. Chem.* **2003**, *24*, 1999−2012.

(30) Frisch, M. J., Trucks, G. W.; Schlegel, H. B.; Scuseria, G. E.; Robb, M. A.; Cheeseman, J. R.; Scalmani, G.; Barone, V.; Mennucci, B.; Petersson, G. A.; Nakatsuji, H.; Caricato, M.; Li, X.; Hratchian, H. P.; Izmaylov, A. F.; Bloino, J.; Zheng, G.; Sonnenberg, J. L.; Hada, M.; Ehara, M.; Toyota, K.; Fukuda, R.; Hasegawa, J.; Ishida, M.; Nakajima, T.; Honda, Y.; Kitao, O.; Nakai, H.; Vreven, T.; Montgomery, Jr., J. A.; Peralta, J. E.; Ogliaro, F.; Bearpark, M.; Heyd, J. J.; Brothers, E.; Kudin, K. N.; Staroverov, V. N.; Kobayashi, R.; Normand, J.; Raghavachari, K.; Rendell, A.; Burant, J. C.; Iyengar, S. S.; Tomasi, J.; Cossi, M.; Rega, N.; Millam, N. J.; Klene, M.; Knox, J. E.; Cross, J. B.; Bakken, V.; Adamo, C.; Jaramillo, J.; Gomperts, R.; Stratmann, R. E.; Yazyev, O.; Austin, A. J.; Cammi, R.; Pomelli, C.; Ochterski, J. W.; Martin, R. L.; Morokuma, K.; Zakrzewski, V. G.; Voth, G. A.; Salvador, P.; Dannenberg, J. J.; Dapprich, S.; Daniels, A. D.; Farkas, Ö.; Foresman, J. B.; Ortiz, J. V.; Cioslowski, J.; Fox, D. J., *Gaussian 09*; Gaussian, Inc.: Wallingford, CT, 2009

(31) Dapprich, S.; Komaromi, I.; Byun, K. S.; Morokuma, K.; Frisch, M. J. *J. Mol. Struct.: THEOCHEM* **1999**, *461*, 1−21.

(32) Maseras, F.; Morokuma, K. *J. Comput. Chem.* **1995**, *16*, 1170−1179.

(33) Becke, A. D. *Phys. Rev. A* **1988**, *38*, 3098−3100.

(34) Becke, A. D. *J. Chem. Phys.* **1996**, *104*, 1040−1046.

(35) Lee, C. T.; Yang, W. T.; Parr, R. G. *Phys. Rev. B* **1988**, *37*, 785−789.

(36) Garrec, J.; Sautet, P.; Fleurat-Lessard, P. *J. Phys. Chem. B* **2011**, *115*, 8545−8558.

(37) Sousa, S. F.; Fernandes, P. A.; Ramos, M. J. *J. Phys. Chem. B* **2007**, *111*, 9146−9152.

(38) Mulholland, A. J. *Chem. Cent. J.* **2007**, *1*, 1 DOI: 10.1186/1752-153X-1-19.

(39) Bras, N. F.; Fernandes, P. A.; Ramos, M. J. *J. Chem. Theory Comput.* **2010**, *6*, 421−423.

(40) Perez, M. A. S.; Fernandes, P. A.; Ramos, M. J. *J. Chem. Theory Comput.* **2010**, *6*, 2770−2781.

(41) Grimme, S.; Antony, J.; Ehrlich, S.; Krieg, H. *J. Chem. Phys.* **2010**, *132*, 154101.

(42) Xu, X.; Goddard, W. A. *Proc. Natl. Acad. Sci. U.S.A.* **2004**, *101*, 2673−2677.

(43) Boese, A. D.; Martin, J. M. L.; Handy, N. C. *J. Chem. Phys.* **2003**, *119*, 3005−3014.

(44) Grimme, S. *J. Comput. Chem.* **2006**, *27*, 1787−1799.

(45) Hamprecht, F. A.; Cohen, A. J.; Tozer, D. J.; Handy, N. C. *J. Chem. Phys.* **1998**, *109*, 6264−6271.
(46) Zhao, Y.; Lynch, B. J.; Truhlar, D. G. *J. Phys. Chem. A* **2004**, *108*, 2715−2719.
(47) Zhao, Y.; Truhlar, D. G. *J. Chem. Phys.* **2006**, *125*, 194101.
(48) Zhao, Y.; Truhlar, D. G. *Acc. Chem. Res.* **2008**, *41*, 157−167.
(49) Zhao, Y.; Truhlar, D. G. *Theor. Chem. Acc.* **2008**, *120*, 215−241.
(50) Zhao, Y.; Schultz, N. E.; Truhlar, D. G. *J. Chem. Theory Comput.* **2006**, *2*, 364−382.
(51) Marino, T.; Russo, N.; Toscano, M. *J. Am. Chem. Soc.* **2005**, *127*, 4242−4253.
(52) Amata, O.; Marino, T.; Russo, N.; Toscano, M. *Phys. Chem. Chem. Phys.* **2011**, *13*, 3468−3477.
(53) Sousa, S. F.; Carvalho, E. S.; Ferreira, D. M.; Tavares, I. S.; Fernandes, P. A.; Ramos, M. J.; Gomes, J. A. N. F. *J. Comput. Chem.* **2009**, *30*, 2752−2763.
(54) Amin, E. A.; Truhlar, D. G. *J. Chem. Theory Comput* **2008**, *4*, 75−85.
(55) Neves, R. P. P.; Sousa, S. F.; Fernandes, P. A.; Ramos, M. J. *J. Chem. Theory Comput* **2013**, *9*, 2718−2732.
(56) Bayly, C. I.; Cieplak, P.; Cornell, W. D.; Kollman, P. A. *J. Phys. Chem.* **1993**, *97*, 10269−10280.
(57) Ryde, U. *Proteins* **1995**, *21*, 40−56.
(58) Ryde, U. *Protein Sci.* **1995**, *4*, 1124−1132.
(59) Ryde, U. *J. Comput. Aided Mol. Design* **1996**, *10*, 153−164.
(60) Case, D. A.; Cheatham, T. E.; Darden, T.; Gohlke, H.; Luo, R.; Merz, K. M.; Onufriev, A.; Simmerling, C.; Wang, B.; Woods, R. J. *J. Comput. Chem.* **2005**, *26*, 1668−1688.
(61) Izaguirre, J. A.; Catarello, D. P.; Wozniak, J. M.; Skeel, R. D. *J. Chem. Phys.* **2001**, *114*, 2090−2098.
(62) Ryckaert, J. P.; Ciccotti, G.; Berendsen, H. J. C. *J. Comput. Phys.* **1977**, *23*, 327−341.
(63) Essmann, U.; Perera, L.; Berkowitz, M. L.; Darden, T.; Lee, H.; Pedersen, L. G. *J. Chem. Phys.* **1995**, *103*, 8577−8593.
(64) Fernandez, M.; Liu, X. F.; Wouters, M. A.; Heyberger, S.; Husain, A. *J. Biol. Chem.* **2001**, *276*, 4998−5004.
(65) Holmes, M. A.; Matthews, B. W. *Biochemistry* **1981**, *20*, 6912−6920.
(66) Oliveira, E. F.; Cerqueira, N.; Fernandes, P. A.; Ramos, M. J. *J. Am. Chem. Soc.* **2011**, *133*, 15496−15505.
(67) Bras, N. F.; Ramos, M. J.; Fernandes, P. A. *J. Mol. Struct.: THEOCHEM* **2010**, *946*, 125−133.
(68) Bras, N. F.; Moura-Tamames, S. A.; Fernandes, P. A.; Ramos, M. J. *J. Comput. Chem.* **2008**, *29*, 2565−2574.
(69) Ribeiro, A. J. M.; Ramos, M. J.; Fernandes, P. A. *J. Am. Chem. Soc.* **2012**, *134*, 13436−13447.
(70) Lonsdale, R.; Harvey, J. N.; Mulholland, A. J. *J. Chem. Theory Comput.* **2012**, *8*, 4637−4645.
(71) Lonsdale, R.; Harvey, J. N.; Mulholland, A. J. *J. Phys. Chem. Lett.* **2010**, *1*, 3232−3237.